Journal of Hydrology 612 (2022) 128042

Contents lists available at ScienceDirect

Journal of Hydrology

journal homepage: www.elsevier.com/locate/jhydrol

Research papers

Assessing future runoff changes with different potential evapotranspiration inputs based on multi-model ensemble of CMIP5 projections

Lijie Shi[a,b,c,d], Puyu Feng[e], Bin Wang[d,*], De Li Liu[d,f], Hong Zhang[c], Jiandong Liu[g,*], Qiang Yu[a,*]

[a] State Key Laboratory of Soil Erosion and Dryland Farming on the Loess Plateau, Northwest A&F University, Yangling, Shaanxi 712100, China
[b] College of Hydraulic Science and Engineering, Yangzhou University, Yangzhou, Jiangsu 225009, China
[c] School of Life Sciences, Faculty of Science, University of Technology Sydney, 15 Broadway, Ultimo NSW 2007, Australia
[d] NSW Department of Primary Industries, Wagga Wagga Agricultural Institute, Pine Gully Road Wagga Wagga, NSW 2650, Australia
[e] College of Land Science and Technology, China Agricultural University, Beijing 100193, China
[f] Climate Change Research Centre and ARC Centre of Excellence for Climate System Science, University of New South Wales, Sydney, NSW 2052, Australia
[g] State Key Laboratory of Severe Weather, Chinese Academy of Meteorological Sciences, Beijing 100081, China

ARTICLE INFO

This manuscript was handled by Emmanouil Anagnostou, Editor-in-Chief

Keywords:
Runoff
Xinanjiang model
Potential evapotranspiration
Climate change
GCMs
Uncertainty

ABSTRACT

Runoff projection under future climate scenarios has been widely studied to investigate the impacts of climate change on regional water availability. However, uncertainty in runoff projection due to different ETp inputs has not been fully assessed. This study firstly adopted the physically-based Penman model, temperature-based Hargreaves model, and radiation-based Abtew, Jensen-Haise, and modified Makkink models to drive Xinanjiang (XAJ) model, thus investigating the influence of different potential evapotranspiration (ETp) inputs on runoff simulation. Then, we used the validated XAJ model to project runoff in North Johnstone catchment, northeast Australia. Lastly, we quantified the uncertainty caused by 34 global climate models (GCMs), different representative concentrative pathway (RCP) scenarios (RCP4.5 & RCP8.5), and different ETp models with the technique of three-way analysis of variance (ANOVA). We found that XAJ model performed well ($R^2 \geq 0.88$, NSE ≥ 0.86) and showed low sensitivity to different ETp inputs in runoff simulation and projection. Under future climate scenarios, spring and winter runoff had a large decrease, which was mainly caused by the decrease in rainfall. The mean decreases in spring and winter runoff were 14.6% – 20.1% and 10.3% – 15.2% respectively by 2090s under RCP8.5. GCMs (50.9% – 67.4%) and their interaction with RCPs (35.4% – 46.6%) were the dominant factors resulting in uncertainty in runoff projection. Our study not only advanced the understanding of the impacts of different ETp inputs on runoff projection but also offered insights on the understanding of the roles different factors played in the uncertainty in runoff projection. We expect such knowledge can provide a way forward to narrow down the uncertainty in runoff projection, thus providing more robust information for policy makers in water management.

1. Introduction

Runoff is one of the key processes in water transport both for surface water bodies (e.g., rivers, lakes, wetlands, and oceans) and groundwater (Ghasemizade and Schirmer, 2013; Kuchment, 2004). The amount of runoff from each rainfall event has direct or indirect influences on water availability in many aspects of human activities such as agricultural and industrial production, and domestic life (Allan et al., 2020; Devi et al., 2015). Previous studies have shown that climate change with increased temperature and changed rainfall patterns has great impacts on runoff (Arnell and Gosling, 2013; Bosshard et al., 2013; Im et al., 2009). For instance, Arnell and Gosling (2013) found that more than 47% of the land surface would experience increases in mean annual runoff whereas around 36% of that would witness mean annual runoff decrease due to changes in temperature and rainfall. Meanwhile, considerable variation in the impact of climate change on runoff has been found among different regions (Arnell and Gosling, 2013; Do et al., 2017; Shen et al., 2014). Providing a robust projection of regional runoff under climate

* Corresponding authors at: State Key Laboratory of Soil Erosion and Dryland Farming on the Loess Plateau, Northwest A&F University, Yangling, Shaanxi 712100, China.
E-mail addresses: bin.a.wang@dpi.nsw.gov.au (B. Wang), Liujd2001@263.net (J. Liu), yuq@nwafu.edu.cn (Q. Yu).

https://doi.org/10.1016/j.jhydrol.2022.128042
Received 27 August 2021; Received in revised form 27 May 2022; Accepted 4 June 2022
Available online 16 June 2022

change plays a significant role in understanding local water resources management and revealing the impacts of a changing climate on local hydrological cycle (Allan et al., 2020; Yan et al., 2020).

Different kinds of methods such as climate elasticity (Xing et al., 2018; Yang and Yang, 2011), Bayesian approach (Freni et al., 2009), and hydrological model (Chiew et al., 2018; Islam et al., 2014) can be used for runoff simulation and projection. Compared with other methods, one of the most important advantages of hydrological models is that they are capable to detect the hydroclimate response to changes by offering a comprehensive and reliable approach at a certain catchment (Guo et al., 2017a; Li et al., 2020). In previous studies, hydrological models were widely used as powerful tools to investigate runoff response to climate change (Fowler et al., 2018; Pechlivanidis et al., 2016; Vaze and Teng, 2011). Specifically, historical observed rainfall and runoff sequences are used to calibrate and validate the performance of hydrological models. Then, runoff can be projected by the calibrated hydrological models forced with the climatic factors derived from global climate models (GCMs) (Arnell, 2011; Chen and Yu, 2015). For instance, Senent-Aparicio et al. (2017) investigated the influence of climate change on runoff in Mediterranean Europe with SWAT model and found that runoff would decrease due to the increase in temperature and decrease in rainfall. In Western Australia, Islam et al. (2014) downscaled climatic data from 11 GCMs under A2 and B1 emission scenarios to drive LUCICAT model for the future rainfall-runoff projection. They found that projected decrease in rainfall would result in a large decrease in runoff for Western Australia in the mid and late of 21st century.

According to closed water balance, runoff for a certain region is roughly the difference between rainfall and actual evapotranspiration (ETa) in a long-term period (Montaldo and Oren, 2018). Therefore, the estimation of ETa is expected to influence the simulation of runoff (Riegger and Tourian, 2014). In the process of runoff simulation with most hydrological models, potential evapotranspiration (ETp) is an essential input to calculate ETa used for simulating runoff (Bai et al., 2016; Li and Zhang, 2017). However, various ETp models generally produce different ETp estimates (Feng et al., 2016; Kumar et al., 1987; Kumar Roy et al., 2020). In this case, which ETp model could produce better runoff simulation is an important question to answer (Dakhlaoui et al., 2020; Oudin et al., 2005; Seiller and Anctil, 2016). In other words, will the difference in ETp estimates result in different runoff simulations/projections? Addressing this question is important in runoff projection under a changing climate as ETp is greatly influenced by future climate (Pan et al., 2015; Zheng et al., 2017).

Oudin et al. (2005) adopted ETp estimated by 27 ETp models to drive four rainfall-runoff hydrological models and investigate the influence of different ETp inputs on historical runoff simulation over 308 catchments across France, Australia, and the United States. They found that these hydrological models showed low sensitivity to ETp inputs but temperature-based and radiation-based ETp models yielded the best runoff simulation. Under future climate scenarios, Seiller and Anctil (2016) assessed the sensitivity of 20 hydrological models in runoff projection to ETp estimated by 24 different equations. They found that the different ETp inputs exerted moderate influence on runoff projection. In Korea, Bae et al. (2011) investigated the sensitivity of three hydrological models to seven ETp methods in runoff projection with downscaled climate data from 13 GCMs. They concluded that the influence of different ETp on runoff projection became larger. On the contrary, Dakhlaoui et al. (2020) found that discharge simulated by three hydrological models was not sensitive to the ETp estimates under different climate conditions. In summary, though studies about the influence of different ETp inputs on future runoff projection are becoming common, there is no consistent conclusion yet.

Another unavoidable challenge in future runoff projection is the uncertainty caused by many factors such as GCMs, hydrological models (Knutti and Sedláček, 2012; Teng et al., 2015), and emission scenarios (Woldemeskel et al., 2016). For instance, Teng et al. (2012) projected runoff based on 15 GCMs with five hydrological models in southeast Australia and found that uncertainty caused by GCMs was much larger than that caused by hydrological models. Vetter et al. (2017) investigated the uncertainty in runoff projection caused by five GCMs, four RCPs, and nine hydrological models across 12 large-scale catchments worldwide. They found that GCMs and RCPs were the main factors resulting in the uncertainty. Similarly, Chegwidden et al. (2019) found that the choice of RCPs or GCMs was the main source influencing the spread in annual streamflow volume and timing. These studies would provide useful information to quantify the dominant source of uncertainty in runoff projection. However, few of them considered the possible contribution of different ETp inputs and their interaction with other factors to the uncertainty in runoff projection. Given that ETp is essential for runoff projection, especially the influence of ETp may become larger under future climate scenarios (Seiller and Anctil, 2016), it is necessary to include ETp in the uncertainty analysis in runoff projection.

Thus, the objectives of this study are dual: 1) to investigate the influence of different ETp inputs both in historical runoff simulation and future runoff projection; 2) to quantify the relative contribution of GCMs, RCPs, ETp models, and their interaction to the uncertainty in runoff projection. To achieve these goals, we calibrated and validated Xinanjiang (XAJ), a rainfall-runoff hydrological model driven by different ETp inputs against observed historical runoff at a humid catchment in northeastern Australia. Then, we used validated XAJ model to project future runoff under RCP4.5 and RCP8.5 with climate data downscaled from 34 GCMs. Based on the projected runoff, we quantified the relative contribution of different factors with the method of analysis of variance. We expect this study can offer further insights into the impacts of different ETp inputs on runoff projection and help to clarify the role of ETp inputs on the related uncertainty. The knowledge from this study will be helpful to guide the ETp model choice in future runoff projection. Results in this study can also provide a way forward to narrow down uncertainty in runoff projection.

2. Materials and methods

2.1. Study area

The study area is North Johnstone catchment (17°16′ S – 17°38′ S, 145°28′ E – 146°40′ E, Fig. 1), locating in the Wet Tropics of Queensland, Australia. It covers an area of 924 km^2, with elevation ranging from 18 m to 1370 m (Zhang et al., 2020). The mean maximum and minimum temperatures in this catchment are around 26.0 °C and 16.7 °C, respectively. Mean annual rainfall in this catchment is around 2530 mm and mean annual runoff is around 1900 mm. The area is influenced by the monsoon and tropical lows/depressions, thus most of its rainfall occurs in austral warmer months from December to May. Specifically, the mean summer (Dec - Feb) and autumn (Mar - May) rainfall is around 1120 mm and 840 mm whereas the mean rainfall in winter (Jun - Aug) and spring (Sep - Nov) is around 300 mm and 270 mm, respectively. Correspondingly, the production of runoff also showed seasonal difference, larger than 70% of runoff yielded in summer and autumn. Fig. 2 showed the seasonal temporal trends of potential evapotranspiration, rainfall, and runoff in North Johnstone catchment in the research period. It showed that rainfall in summer and autumn is generally higher than evapotranspiration whereas spring and winter rainfall were lower than evapotranspiration. In other words, spring and winter are relatively drier than summer and autumn in this region.

Pasture and conserved natural rainforest are the main vegetation types of the catchment. The area of pasture and conserved natural rainforest cover 51% and 37% of the catchment, respectively (Rafiei et al., 2020). Banana, sugarcane, tea, and tropical fruit are the main agricultural product in the catchment. Meanwhile, runoff from this catchment is one of the water sources running to the Great Barrier Reef (GBR). Thus, changes in runoff here may have an influence on the ecological function of GBR.

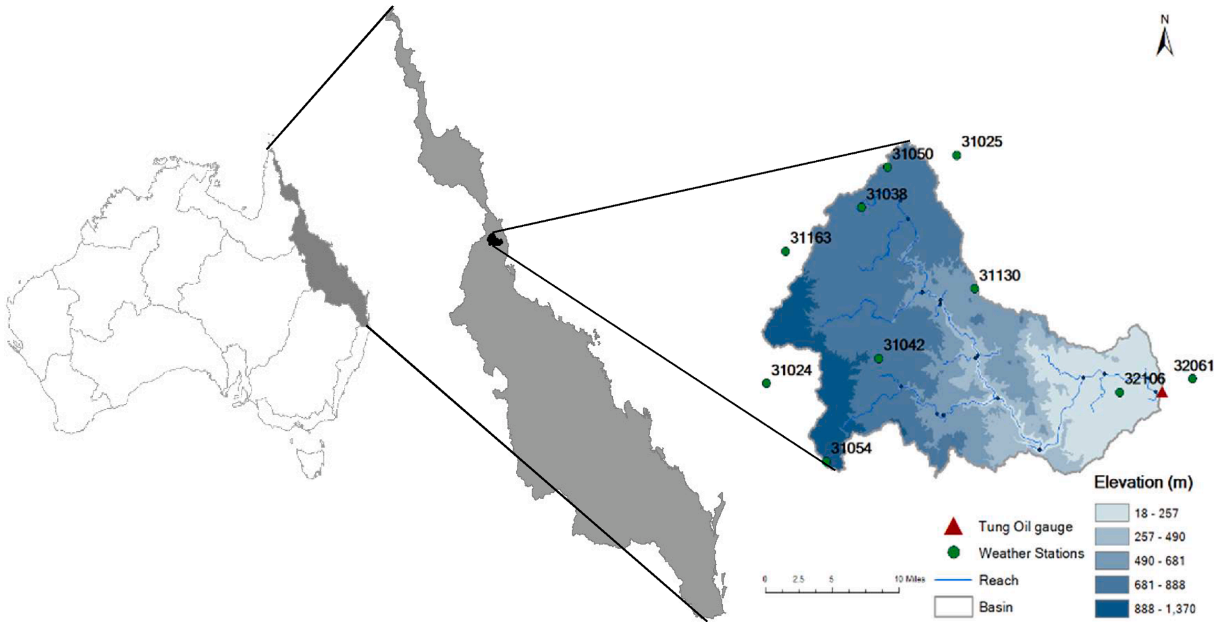

Fig. 1. Location of the North Johnstone River catchment, Queensland, Australia and the distribution of 10 weather stations and the location of Tung Oil gauge (a hydrologic gauge station).

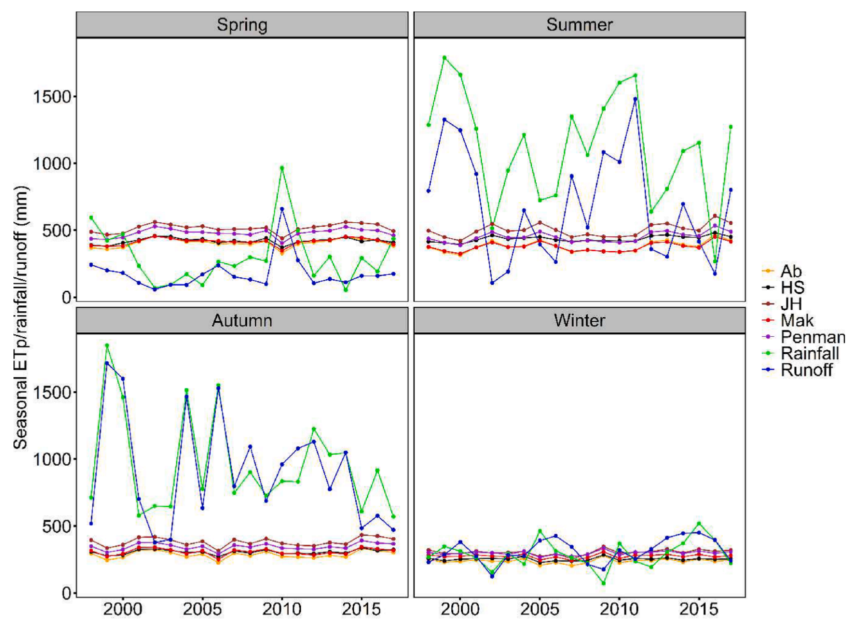

Fig. 2. Seasonal ETp estimated by Ab, HS, JH, Mak, and Penman models, and seasonal rainfall and runoff in North Johnstone catchment from 1998 to 2017.

2.2. Observed historical climatic data and downscaled future climatic data

Historical daily climatic data from ten weather sites (Fig. 1) within or near by the catchment was extracted from the Scientific Information for Land Owners (SILO) patched point dataset (https://www.longpaddock.qld.gov.au/silo/datadrill/index.php) (Jeffrey et al., 2001). These data included maximum temperature (T_{max}), minimum temperature (T_{min}), maximum relative humidity (RH_{max}), minimum relative humidity (RH_{min}), solar radiation (R_s), and rainfall. On the one hand, they were used to estimate historical ETp and drive Xinanjiang model for historical runoff simulation. On the other hand, they were used to do second bias correction for GCMs output as a part of the statistical downscaling procedure.

Monthly T_{max}, T_{min}, R_s, and rainfall under RCP4.5 and RCP8.5 were downscaled from 34 GCMs grids to these ten sites with the method developed by Liu and Zuo (2012). In detail, the monthly gridded climate data from GCMs were firstly interpolated to the ten sites with inverse distance-weighted interpolation method. Then, bias correction was carried out to correct the stationary bias and systemic errors embedded with the site-specific monthly GCM projections against SILO historical data. Lastly, daily climatic data at these sites were generated using a stochastic weather generator (Liu and Zuo, 2012). The detailed information about the 34 GCMs can be referred to Shi et al. (2020).

These downscaled climate data were used to estimate ETp under climate change scenarios. Then, the ETp and downscaled rainfall were used in XAJ model as inputs for runoff projection. In theory, the downscaled climate data from GCMs would be comparable to the observed ones if the bias correction in the second step was perfect during the downscaling procedure. Thus, the projected runoff with downscaled climate data was also expected to be similar to those of an otherwise identically simulated with observations. However, as the bias correction in the second step mainly works for stationary bias and systemic errors (e.g., mean bias and projected trends in the future), and fails in correcting the bias caused by misrepresentation of dynamical (physical) processes or non-stationary biases caused by GCMs (Haerter et al., 2011; Yang et al., 2016). In other words, the runoff projected with downscaled climate data is not likely to be as the same as the one of an otherwise identically simulated with observations. The difference between runoff projected with downscaled GCM data and runoff identically simulated with observations can be viewed as biophysical biases. In this study, we adopted a secondary bias-correction method (Yang et al., 2016) to correct the multi-year averages of projected runoff with the following equation.

$$Roff = Roff_G - (\overline{Roff_{Gbl}} - \overline{Roff_{Obl}}) \tag{1}$$

where R*off* is the projected value after the second bias-correction; $Roff_G$ is the projected value from XAJ model driven by downscaled climate data; $\overline{Roff_{Gbl}}$ is the mean projected runoff over a historical baseline period with downscaled climate data; $\overline{Roff_{Obl}}$ is the corresponding mean runoff over the historical period with observed climate data.

2.3. Empirical ETp models

Air temperature and solar radiation are two key factors influencing ETp. It's reported that they can explain about 80% of variations in ETp (Almorox et al., 2015; Priestley and Taylor, 1972; Samani, 2000). Meanwhile, compared with other climatic factors (e.g. wind speed), air temperatures downscaled from GCMs are more reliable under future climate scenarios (Guo et al., 2017b). Furthermore, Oudin et al. (2005) reported that temperature-based ETp models can produce reliable runoff simulation. Therefore, this study adopted both the physically-based Penman model, the commonly used temperature-based Hargreaves (HS), and radiation-based models including Jensen-Haise (JH), Abtew (Ab), and modified Makkink (Mak) to investigate the influence of different ETp inputs on runoff simulation. Their performance in estimating ETp has been demonstrated in Shi et al. (2020). The mathematical expressions of these empirical ETp models were shown in the following equations.

The physical-based Penman model:

$$ETp_{,\,\mathrm{Penman}} = \frac{0.408\Delta}{\Delta+\gamma}(R_n - G) + \frac{\gamma}{\Delta+\gamma}\frac{6.43(1+0.536u_2)(e_s - e_a)}{\lambda} \tag{2}$$

where R_n (MJ m^{-2} day^{-1}) is the net radiation determined by the difference between the net solar (shortwave) radiation (R_{ns}, MJ m^{-2} day^{-1}) and the net longwave radiation (R_{nl}, MJ m^{-2} day^{-1}) (Allen et al., 1998), as shown in equation (3). G (MJ m^{-2} day^{-1}) is soil heat flux density, zero for periods of a day or longer (Allen et al., 1998; Irmak et al., 2012); u_2 (m s^{-1}) is wind speed at 2 m height; e_s (kPa) is saturation vapor pressure; e_a (kPa) is actual vapor pressure; (e_s-e_a) (kPa) is saturation vapor pressure deficit; $\triangle$ (kPa $^\circ C^{-1}$) is the slope of the vapor pressure curve; γ (kPa $^\circ C^{-1}$) is the psychrometric constant; and λ is the latent heat of vaporization of water, 2.45 MJ kg^{-1} at 20 °C.

$$R_n = R_{ns} - R_{nl} \tag{3}$$

where the net solar (shortwave) radiation (R_{ns}, MJ m^{-2} day^{-1}) and the net longwave radiation (R_{nl}, MJ m^{-2} day^{-1}) is estimated by the following equation (4) and equation (5), respectively.

$$R_{ns} = (1-\alpha)R_s \tag{4}$$

where R_s (MJ m^{-2} day^{-1}) is measured solar radiation extracted from SILO; α is albedo, varying from 0.20 to 0.25 for green vegetation cover. This study adopted the FAO recommended value, 0.23 (Allen et al., 1998).

$$R_{nl} = 4.903\times10^{-9}\times\frac{(T_{max}+273.06)^4+(T_{min}+273.06)^4}{2}\times(0.34 - 0.14\sqrt{e_a})\times\left(1.35\times\frac{R_s}{R_{so}}-0.35\right) \tag{5}$$

where T_{max} (°C) is maximum air temperature; T_{min} (°C) is minimum air temperature; e_a (kPa) is actual vapor pressure; R_{so} (MJ m^{-2} day^{-1}) is clear-sky radiation, which is estimated by the station elevation and extraterrestrial radiation.

The radiation-based models:

$$ETp_{,JH} = 0.0102(T+3)R_s \tag{6}$$

$$ETp_{,Ab} = 0.01786\frac{R_sT_{\max}}{\lambda} \tag{7}$$

$$ETp_{,Mak} = 0.7\frac{\Delta}{\Delta+\gamma}\frac{R_s}{\lambda} \tag{8}$$

Parameters in these equations have the same meaning with that in Penman model.

The temperature-based model:

$$ETp_{,HS} = 0.0023\times0.408R_a(T_{\max}-T_{\min})^{0.5}(T+17.8) \tag{9}$$

where R_a (MJ m^{-2} day^{-1}) is extraterrestrial radiation, estimated from equation (10); T_{max}, T_{min}, and T (°C) are maximum, minimum, and mean air temperatures, respectively.

$$R_a = \frac{24(60)}{\pi}G_{sc}d_r[\omega_s\sin(\varphi)\sin(\delta)+\cos(\varphi)\cos(\delta)\sin(\omega_s)] \tag{10}$$

where G_{sc} is solar constant, 0.0820 MJ m^{-2} min^{-1}, d_r is inverse relative distance Earth-Sun; ω_s(rad) is sunset hour angle; φ(rad) is station latitude; δ(rad) is solar declination. d_r and δ are determined by the number of the day in the year while ω_s is a function of φ andδ. More details about the calculation of these parameters can be referred to Allen et al. (1998).

2.4. Xinanjiang (XAJ) model

As a lumped conceptual rainfall-runoff hydraulic model, the XAJ model has been widely used to simulate runoff in humid and sub-humid regions (Li et al., 2012; Zhang et al., 2019). Due to the consistent performance of XAJ model in runoff simulation, it also has been widely used to investigate the response of runoff to climate change (Seiller and Anctil, 2014; Tian et al., 2013). XAJ model is divided into four submodels, namely a three-layer evapotranspiration sub-model, runoff production sub-model, separation of runoff components sub-model, and flow concentration sub-model (Zhang et al., 2019; Zhao, 1992). Fig. 3 and Table 1 showed the flow chart and 16 parameters used in XAJ model, respectively. The area-mean daily rainfall and ETp are inputs for this model and daily runoff and ETa are the outputs. The runoff simulated by XAJ model is based on the assumption that runoff is produced after the soil moisture content of the aeration zone has reached field capacity (Zhao, 1992).

2.5. Calibration and validation of XAJ model and scenario analysis

The calculated ETp and the observed rainfall at all ten sites were used to calculate the area-mean ETp and area-mean rainfall to drive XAJ model for runoff simulation. Historical daily observed discharge from the Tung Oil gauge, which received most of the streamflow from the catchment was extracted from the Bureau of Meteorology website (https://www.bom.gov.au/waterdata/) were used to calibrate and validate XAJ model.

The historical climatic data from 1998 to 2010 were used to calibrate

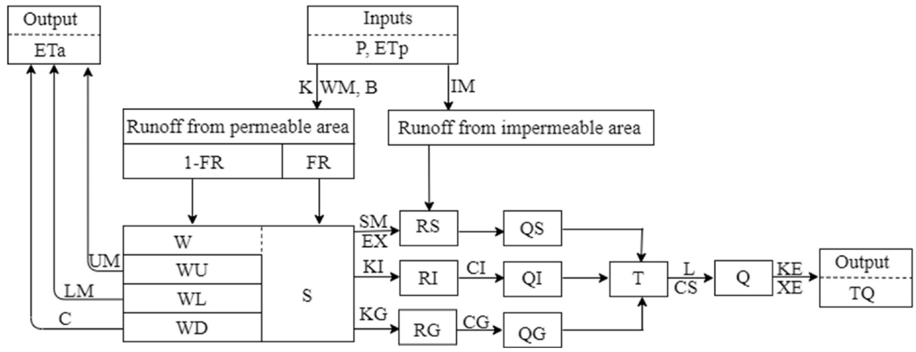

Fig. 3. The structure layers of the XAJ model.

Table 1
The 16 parameters used in XAJ model to simulate runoff.

Layers	Parameters	Meaning of parameters (units)
Evapotranspiration	UM	Areal mean tension water capacity in the upper layer (mm)
	LM	Areal mean tension water capacity in the lower layer (mm)
	C	Coefficient of deep evapotranspiration
Runoff production	WM	Areal mean tension water capacity (mm)
	B	Exponent of the tension water capacity (mm)
	IM	Ratio of the impervious to the total area of the basin
Separation of runoff components	SM	Areal mean of the free water capacity of the surface soil layer (mm)
	EX	Exponent of the free water capacity curve
	KG	Outflow coefficient of the free water storage to groundwater
	KI	Outflow coefficient of the free water storage to interflow
Flow concentration	CI	Recession constant of the interflow storage
	CG	Recession constant of groundwater storage
	CS	Recession constant of surface water storage
	L	Lay time (day)
	KE	Parameters of the Muskingum method (h)
	XE	Parameters of the Muskingum method

XAJ model while the data from 2011 to 2017 were used for model's validation. This study used SCE-UA (Shuffled Complex Evolution method developed at the University of Arizona), a global optimization method to optimize XAJ model parameters (Zhang et al., 2019). Firstly, individual ETp model was used to calculate ETp and drive XAJ model. Then, the parameters calibrated by a certain ETp model were used to validate XAJ model for other ETp models in addition to the one used for calibration. In other words, cross-model validation was carried out among these ETp models to investigate the sensitivity of XAJ model to different ETp inputs. Then, the group of parameters that produced the best runoff simulation for all ETp models were used in runoff projections with downscaled climatic data under future climate scenarios. The empirical models including JH, Ab, Mak, and HS were used to project future runoff in order to investigate the influence of different ETp models on runoff projection.

Nash-Sutcliffe Efficiency (NSE), coefficient of determination (R^2), and root mean square error (RMSE) were used to evaluate the performance of the XAJ model driven by different models-estimated ETp against observed runoff. The NSE has been widely used in comparing hydrologic model performance (Fang et al., 2020; Li et al., 2009). It ranges from -∞ to 1. The value of 1 represents that the model-simulated runoff perfectly matches with the observed runoff. Therefore, the closer the NSE value is to 1, the better the hydrological model performs. Generally, a hydrological model with NSE and R^2 larger than 0.50 is capable of effectively simulating stream flow for a certain catchment (Zhang et al., 2019). The NSE, R^2, and RMSE were calculated with the following equations:

$$NSE = 1 - \frac{\sum_{i=1}^{N}\left(Q_{obs,i} - Q_{sim,i}\right)^2}{\sum_{i=1}^{N}\left(Q_{obs,i} - \overline{Q_{obs}}\right)^2} \tag{11}$$

$$R^2 = \frac{\left[\sum_{i=1}^{N}\left(Q_{obs,i} - \overline{Q_{obs}}\right)\left(Q_{sim,i} - \overline{Q_{sim}}\right)\right]^2}{\sum_{i=1}^{N}\left(Q_{obs,i} - \overline{Q_{obs}}\right)^2\sum_{i=1}^{N}\left(Q_{sim,i} - \overline{Q_{sim}}\right)^2} \tag{12}$$

$$RMSE = \sqrt{\frac{1}{n}\sum_{i=1}^{n}\left(Q_{\mathrm{obs},i} - Q_{sim}\right)^2} \tag{13}$$

where $Q_{obs,i}$ (mm day^{-1}) was the observed runoff for *i*-th day; $Q_{sim,i}$ (mm day^{-1}) was simulated runoff for *i*-th day,; $\overline{Q_{obs}}$ (mm day^{-1}) and $\overline{Q_{sim}}$ (mm day^{-1}) are the corresponding mean daily values of observed runoff and simulated runoff in the research period.

To project the change of runoff in the future period, we divided the downscaled climatic data into five time periods, namely baseline period from 1998 to 2017; near future period from 2021 to 2040 (2030s); middle future period from 2041 to 2060 (2050s); far future period from 2061 to 2080 (2070s); and further future period from 2081 to 2100 (2090s).

2.6. Partitioning uncertainty to different sources

Analysis of variance (ANOVA) method is capable of separating the total observed variances into different sources and considering the interactive contributions of different sources (Bosshard et al., 2013; Lee et al., 2021). In other words, one of the advantages of ANOVA method is that it quantifies both uncertainty related to each source and uncertainty related to the interaction among different sources (Morim et al., 2019; Yip et al., 2011). Interaction effects in ANOVA represent the combined effects of factors on the dependent variable. Thus, this method has been widely used in uncertainty analysis in climate change impact assessment (Lee et al., 2021; Morim et al., 2019; Wang et al., 2020a). For instance, Yip et al. (2011) adopted ANOVA method to quantify the total uncertainty in climate projections into uncertainties related to GCMs, RCPs, and their interaction. Morim et al. (2019) adopted a three-way ANOVA method to quantify the uncertainty in wind-wave climate projections related to GCMs, RCPs, and different wave modelling methods. GCMs, RCP scenarios (RCP4.5 and RCP8.5 for 2030s, 2050s, 2070s, and 2090s, respectively), and ETp models are the sources contributing to the uncertainty for runoff projection in our study. Accordingly, we adopted a three-way ANOVA method and varied the 34 GCMs, 4 ETp models, and 8 RCP scenarios (RCP4.5_2030s, RCP4.5_2050s, RCP4.5_2070s, RCP4.5_2090s, RCP8.5_2030s, RCP8.5_2050s, RCP8.5_2070s, and RCP8.5_2090s) in all possible combinations (which is 1088 subsets in total) to analyze the relative and interactive contribution of these sources. That is, the ANOVA was fit based on the projected mean seasonal runoff *x(g, r, e)* for the *g-th* GCM, *r-th* RCP scenarios, and *e-th* ETp model. Equation (14) to Equation (29) showed the calculation of total sum of squares and squares due to individual effects and interactive effects. The calculation was conducted with the *aov()* function of R software.

$$SST = \underbrace{SS_{GCMs} + SS_{RCPs} + SS_{ETp,models}}_{main\ effects} + \underbrace{SS_{GCMs:RCPs} + SS_{GCMs:ETp,models} + SS_{RCPs:ETp,models} + SS_{GCMs:RCPs:ETp,models}}_{interaction\ effects} \tag{14}$$

where SS_{GCMs}, SS_{RCPs}, and $SS_{ETp,models}$ represents the variance due to GCMs, RCPs, and ETp models, respectively; $SS_{GCMs:RCPs}$, $SS_{GCMs:ETp,models}$, $SS_{RCPs:ETp,models}$, and $SS_{GCMs:RCPs:ETp,models}$ represents the variance due to the interaction among GCMs, RCPs, and ETp models.

$$SST = \sum_{g=1}^{N_g}\sum_{r=1}^{N_r}\sum_{e=1}^{N_e}[x(g,r,e) - x(\cdot,\cdot,\cdot)]^2 \tag{15}$$

$$SS_{GCMs} = N_rN_e\sum_{g=1}^{N_g}[(x(g,\cdot,\cdot) - x(\cdot,\cdot,\cdot))]^2 \tag{16}$$

$$SS_{RCPs} = N_gN_e\sum_{r=1}^{N_r}[(x(\cdot,r,\cdot) - x(\cdot,\cdot,\cdot))]^2 \tag{17}$$

$$SS_{ETp,\ models} = N_gN_r\sum_{e=1}^{N_e}[(x(\cdot,\cdot,e) - x(\cdot,\cdot,\cdot))]^2 \tag{18}$$

$$x(g,\cdot,\cdot) = \frac{1}{N_rN_e}\sum_{r=1}^{N_r}\sum_{e=1}^{N_e}x(g,r,e) \qquad g = 1,\dots,N_g \tag{24}$$

$$x(\cdot,r,\cdot) = \frac{1}{N_gN_e}\sum_{g=1}^{N_g}\sum_{e=1}^{N_e}x(g,r,e) \quad \mathrm{r} = 1,\dots,\mathrm{N}_r \tag{25}$$

$$x(\cdot,\cdot,e) = \frac{1}{N_gN_r}\sum_{g=1}^{N_g}\sum_{r=1}^{N_r}x(g,r,e) \quad \mathrm{e} = 1,\dots,\mathrm{N}_e \tag{26}$$

$$x(g,r,\cdot) = \frac{1}{N_e}\sum_{e=1}^{N_e}x(g,r,e) \quad \mathrm{g} = 1,\dots,\mathrm{N}_g,\ \mathrm{r} = 1,\dots,\mathrm{N}_r \tag{27}$$

$$x(g,\cdot,e) = \frac{1}{N_r}\sum_{r=1}^{N_r}x(g,r,e) \quad \mathrm{g} = 1,\dots,\mathrm{N}_g,\ \mathrm{e} = 1,\dots,\mathrm{N}_e \tag{28}$$

$$x(\cdot,r,e) = \frac{1}{N_g}\sum_{g=1}^{N_g}x(g,r,e) \quad \mathrm{r} = 1,\dots,\mathrm{N}_r,\ \mathrm{e} = 1,\dots,\mathrm{N}_e \tag{29}$$

where Ng, Nr, and Ne are the numbers of GCMs, RCP scenarios, and ETp models, respectively.

After calculating the total sum square and sum squares for each uncertainty source, the relative contribution of each uncertainty source was calculated as the proportion of the partial variances (SS) to the total sum of the variances (SST).

3. Results

3.1. Calibration and validation of the XAJ model

As one of the key inputs in runoff simulation, difference was observed in ETp estimated by different models (Figure S1). For instance,

$$\begin{aligned} SS_{GCMs:RCPs} &= N_e\sum_{g=1}^{N_g}\sum_{r=1}^{N_r}\langle x(g,r,\cdot) - \{x(\cdot,\cdot,\cdot) + [x(g,\cdot,\cdot) - x(\cdot,\cdot,\cdot)] + [x(\cdot,r,\cdot) - x(\cdot,\cdot,\cdot)]\}\rangle^2 \\ &= \mathrm{N}_e\sum_{g=1}^{N_g}\sum_{r=1}^{N_r}[x(g,r,\cdot) - x(g,\cdot,\cdot) - x(\cdot,r,\cdot) + x(\cdot,\cdot,\cdot)]^2 \end{aligned} \tag{19}$$

$$\begin{aligned} SS_{GCMs:ETp,\ models} &= N_r\sum_{g=1}^{N_g}\sum_{e=1}^{N_e}\langle x(g,\cdot,e) - \{x(\cdot,\cdot,\cdot) + [x(g,\cdot,\cdot) - x(\cdot,\cdot,\cdot)] + [x(\cdot,\cdot,e) - x(\cdot,\cdot,\cdot)]\}\rangle^2 \\ &= \mathrm{N}_r\sum_{g=1}^{N_g}\sum_{e=1}^{N_e}[x(g,\cdot,e) - x(g,\cdot,\cdot) - x(\cdot,\cdot,e) + x(\cdot,\cdot,\cdot)]^2 \end{aligned} \tag{20}$$

$$\begin{aligned} SS_{RCPs:ETp,models} &= N_g\sum_{r=1}^{N_r}\sum_{e=1}^{N_e}\langle x(\cdot,r,e) - \{x(\cdot,\cdot,\cdot) + [x(\cdot,r,\cdot) - x(\cdot,\cdot,\cdot)] + [x(\cdot,\cdot,e) - x(\cdot,\cdot,\cdot)]\}\rangle^2 \\ &= \mathrm{N}_g\sum_{r=1}^{N_r}\sum_{e=1}^{N_e}[x(\cdot,r,e) - x(\cdot,r,\cdot) - x(\cdot,\cdot,e) + x(\cdot,\cdot,\cdot)]^2 \end{aligned} \tag{21}$$

$$\begin{aligned} SS_{GCMs:RCPs:ETp,models} &= SST - SS_{GCMs} - SS_{RCPs} - SS_{ETp,models} \\ &- SS_{GCMs:RCPs} - SS_{GCMs:ETp,models} - SS_{RCPs:ETp,models} \end{aligned} \tag{22}$$

where.

$$x(\cdot,\cdot,\cdot) = \frac{1}{N_gN_rN_e}\sum_{g=1}^{N_g}\sum_{r=1}^{N_r}\sum_{e=1}^{N_e}x(g,r,e) \tag{23}$$

more ETp estimated by Ab was lower than 4 mm day^{-1} whereas JH estimated ETp were more likely to be higher than 4 mm day^{-1}. However, the observed runoff and simulated runoff from the XAJ model (driven by different ETp inputs) did not show great difference, as indicated by similar R^2 (Fig. 4, top panel), NSE (Fig. 4, middle panel), and RMSE (Fig. 4, bottom panel) both in calibration and validation periods. Take the validation period as an explanation, R^2, NSE, and RMSE ranged from 0.88 to 0.89, 0.86 to 0.88, and from 2.74 mm day^{-1} to 2.90 mm day^{-1}, respectively. The high R^2 and NSE indicated that XAJ model was capable

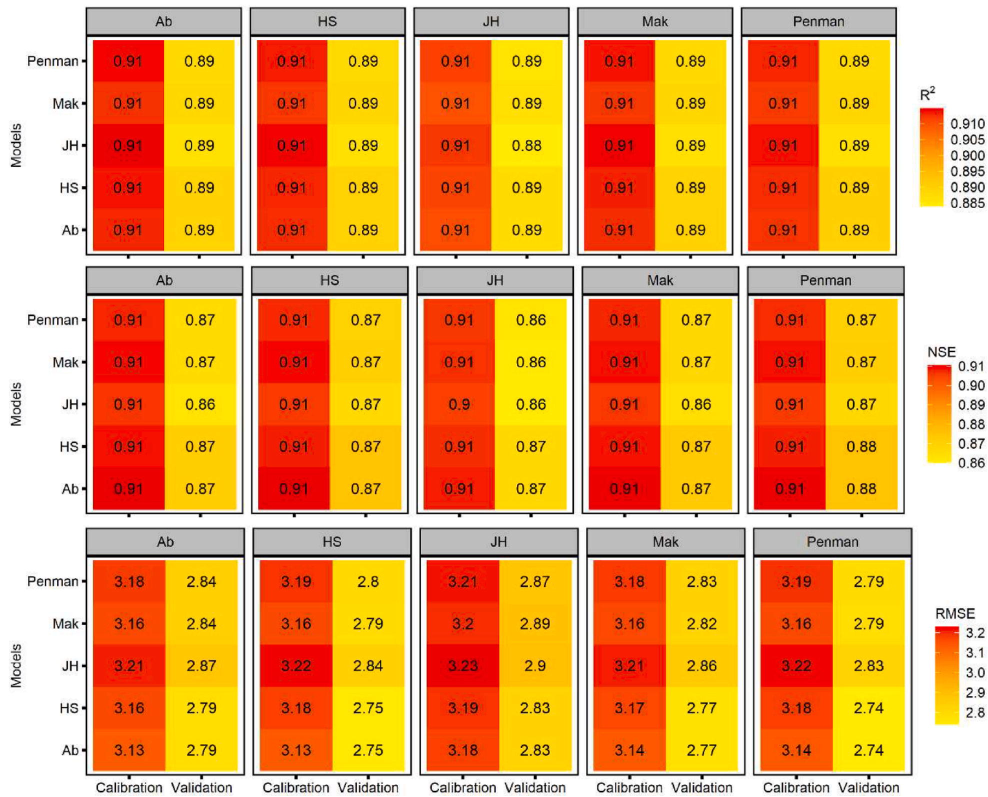

Fig. 4. The R^2, NSE, and RMSE (mm day^{-1}) between observed and simulated runoff with the five groups of parameters are shown in Table 2. The cross-model validation method was used to calibrate XAJ model.

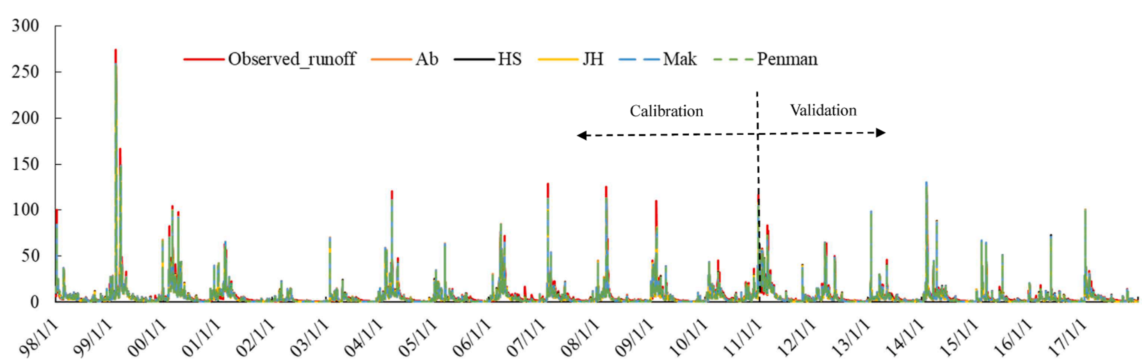

Fig. 5. The observed daily runoff and the simulated daily runoff by XAJ model with calibrated parameters of Ab model (as in Table 2, marked with red) during calibration (1998–2010) and validation (2011–2017) periods in the North Johnstone catchment.

to simulate observed runoff very well. Meanwhile, the results suggested that ETp models (i.e. Penman model) which had more complicated structures were not always likely to outperform the simple empirical models in runoff simulation. Fig. 5 showed the daily runoff temporal trends from 1998 to 2017. It showed that temporal trends of observed runoff were well replicated by XAJ model regardless of the ETp inputs. This finding also confirmed that the difference of ETp inputs had little influence on the runoff simulation.

3.2. Changes in rainfall and potential evapotranspiration under future climate scenarios

Compared with the baseline period (1998–2017), the change of rainfall under future climate scenarios showed seasonal difference (Fig. 6). In general, the decreases in spring and winter rainfall were higher than that in summer and autumn. The mean decreases for spring rainfall ranged from 2.% to 3.5% under RCP4.5 and from 5.3% to 11.1% under RCP8.5. The corresponding mean decreases for winter rainfall ranged from 3.4% to 8.8% and from 6.2% to 7.1%, respectively.

Contrary to the decreases in seasonal rainfall, all seasonal ETp would increase in the future (Fig. 7). The magnitudes of increases showed variation among ETp models. Specifically, JH and Ab generally projected higher increases in ETp than HS and Mak did. Another pattern showed by ETp increases was that the increases under RCP8.5 were higher than that under RCP4.5. Meanwhile, the increases of ETp also became higher with the time getting into the further future periods. The mean increases of spring ETp projected by JH (Ab) varied from 1.9% (1.8%, 2030s) to 8.0% (6.4%, 2090s) under RCP4.5 while Mak (HS) projected increases ranged from 0.7% (0.3%, 2030s) to 3.0% (3.5%, 2090s). Under RCP8.5, the JH (Ab) projected increases ranged from 3.0% (2.9%, 2030s) to 16.5% (13.1%, 2090s) and Mak (HS) projected increases ranged from 1.3% (0.8%, 2030s) to 5.1% (7.1%, 2090s).

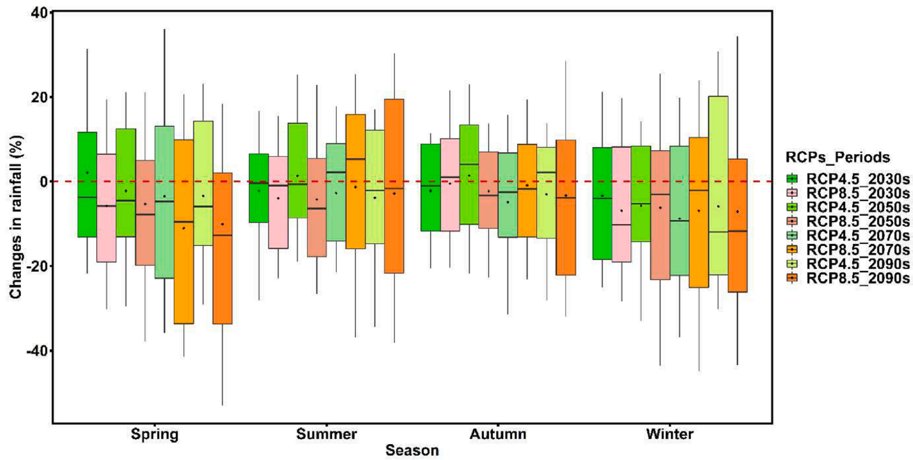

Fig. 6. Projected seasonal changes in rainfall (%) in the North Johnstone catchment in the near (2021–2040, 2030s), middle (2041–2060, 2050s), far (2061–2080, 2070s), and further future periods (2081–2100, 2090s) under RCP4.5 and RCP8.5 scenarios based on 34 GCMs compared with the baseline period (1998–2017). The upper and lower box boundaries indicate the 75th and 25th percentiles; the black line and the black dot within the box represents the median and mean values, respectively; the upper and lower whiskers are the 10th and 90th percentiles.

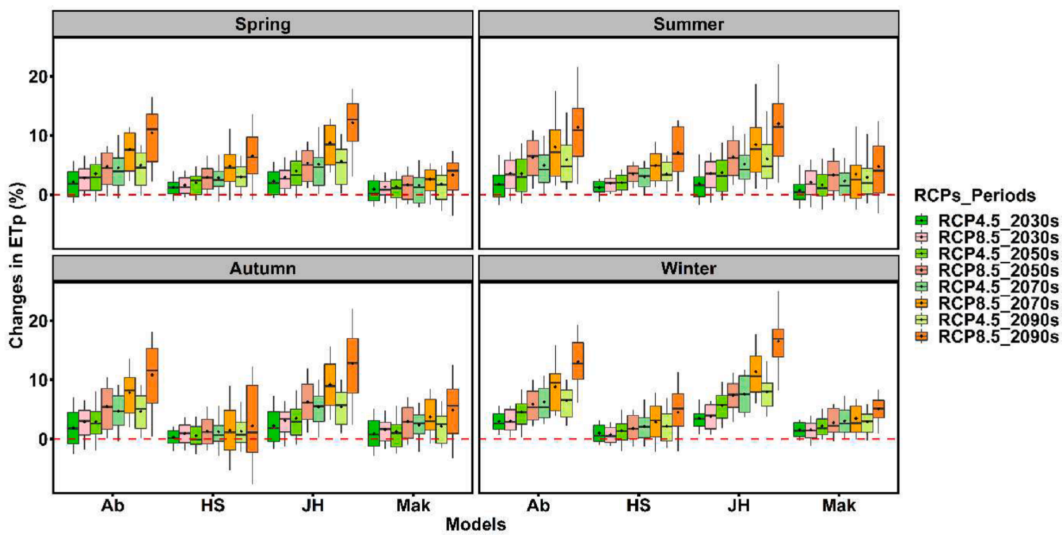

Fig. 7. Projected seasonal changes in ETp (%) in the North Johnstone catchment in the near (2021–2040, 2030s), middle (2041–2060, 2050s), far (2061–2080, 2070s), and further future periods (2081–2100, 2090s) under RCP4.5 and RCP8.5 scenarios based on 34 GCMs compared with the baseline period (1998–2017). The upper and lower box boundaries indicate the 75th and 25th percentiles; the black line and the black dot within the box represents the median and mean values, respectively; the upper and lower whiskers are the 10th and 90th percentiles.

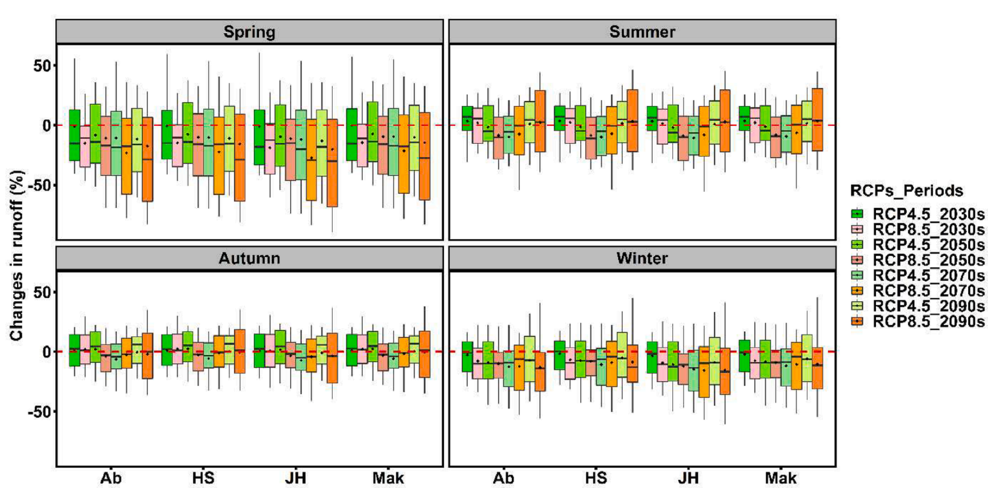

Fig. 8. Projected seasonal changes in runoff (%) with different ETp inputs in the North Johnstone catchment in the near (2021–2040, 2030s), middle (2041–2060, 2050s), far (2061–2080, 2070s), and further future periods (2081–2100, 2090s) under RCP4.5 and RCP8.5 scenarios based on 34 GCMs compared with the baseline period (1998–2017). The upper and lower box boundaries indicate the 75th and 25th percentiles; the black line and the black dot within the box represents the median and mean values, respectively; the upper and lower whiskers are the 10th and 90th percentiles.

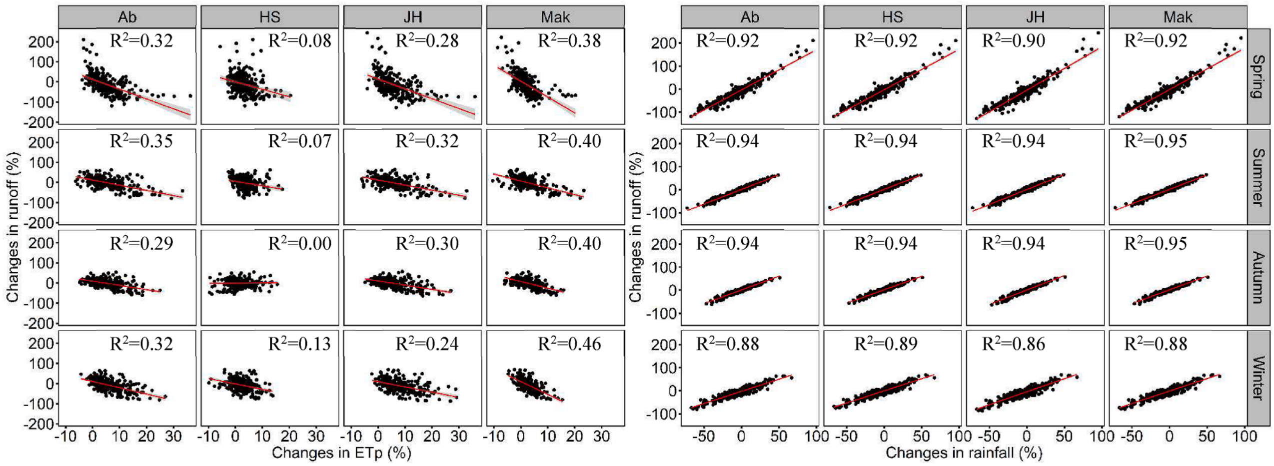

Fig. 9. The relationship between changes in simulated seasonal runoff and changes in ETp and rainfall.

3.3. Changes in runoff under future climate scenarios

The changes of runoff under future climate scenarios with different ETp inputs were shown in Fig. 8. We found that the seasonal difference of changes in runoff was similar to that in rainfall. In other words, spring and winter runoff generally showed larger decreases than that in summer and autumn. Furthermore, runoff would generally experience larger decreases under RCP8.5 than that under RCP4.5 for the same future period. For example, XAJ model with all ETp inputs projected a slight decrease (around 0.7%) in spring runoff under RCP4.5 by 2030s whereas the decrease was around 15.7% under RCP8.5. By 2090s, the decrease of spring runoff projected with different ETp inputs ranged from 10.1% (Mak) to 13.1% (JH) under RCP4.5 and from 14.6% (Mak) to 20.1% (JH) under RCP8.5. The mean decreases of winter runoff varied from 2.1% (Mak) to 3.4% (JH) by 2030s and from 5.9% (Mak) to 8.9% (JH) by 2090s under RCP4.5. The corresponding decreases under RCP8.5 were 7.4% (Mak) −9.3% (JH) by 2030s and 10.3% (Mak) −15.2% (JH) by 2090s.

To investigate the relationship between changes in runoff and changes in rainfall and ETp, the scatter plots between them were shown in Fig. 9. The R^2 between changes in runoff and ETp was not larger than 0.46 whereas the R^2 between changes in runoff and rainfall was no less than 0.86. This finding indicated that changes in runoff were mainly caused by changes in rainfall.

3.4. Uncertainty in runoff projection

Fig. 10 displayed the relative contribution of different sources to the uncertainty caused in runoff projection for each season. GCMs generally contributed the most to the uncertainty, ranging from 50.9% to 67.4%. The interaction between GCMs and RCPs also played a significant role in the total uncertainty, ranging from 35.4% to 46.6%. In contrast, the uncertainty caused by different ETp models was minor for all seasons, even though it was getting larger in winter than that in spring. The minor role of ETp models may be explained by the fact that runoff projection via XAJ model was rarely influenced by the difference of ETp models, as shown in Fig. 8 and Fig. 9.

4. Discussion

4.1. Low sensitivity of XAJ model to different ETp inputs

Compared with XAJ model driven by physically-based Penman calculated ETp, it showed comparable (or even better) ability in runoff simulation with temperature-based (HS) and radiation-based ETp inputs. For instance, with the same R^2 and NSE, RMSE produced by XAJ model with Penman-ETp was even larger (0.05 mm day^{-1}) than that produced by XAJ model with Ab and HS ETp inputs (Fig. 4). In spite of the small difference among different ETp inputs, XAJ model performed well in reproducing daily observed runoff (Fig. 5), with R^2 larger than 0.88, NSE larger than 0.86, and RMSE less than 3.23 mm day^{-1} (Fig. 4).

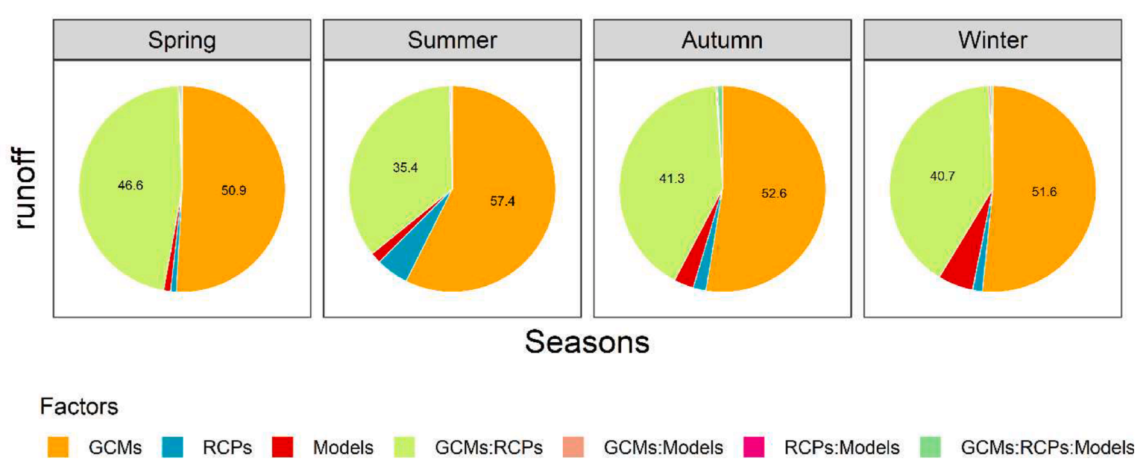

Fig. 10. The relative contribution of GCMs, RCPs, ETp models, and their interactions to the total uncertainty in runoff projections for each season in the North Johnstone catchment.

Table 2
Five groups of parameters calibrated with different ETp inputs estimated by different models to drive XAJ model. The group of parameters marked with red was used for future runoff simulation.

	Ab	HS	JH	Mak	Penman
WUM	10	10	10	10	10
WLM	90	90	90	90	90
C	0.0461	0.0567	0.026	0.0292	0.02
WM	120	120	120	120	120
B	0.35	0.35	0.35	0.35	0.35
IM	0.0399	0.04	0.04	0.04	0.0399
SM	52	60	53	53	53
EX	1.1057	1.3508	1.3873	1.1607	1.0363
KG	0.3001	0.3001	0.3002	0.3	0.3001
KI	0.4997	0.4501	0.4998	0.5	0.4988
CI	0.8383	0.843	0.825	0.8381	0.8411
CG	0.9805	0.9824	0.9854	0.9818	0.9839
CS	0.1	0.1	0.1	0.1	0.1
L	0	0	0	0	0
KE	24	24	24	24	24
XE	0.2923	0.1603	0.1286	0.3536	0.2517

Under future climate scenarios, runoff projected with different ETp inputs also showed similar change patterns (Fig. 8). These findings demonstrated the low sensitivity of XAJ model to different ETp inputs. Similar results were also reported in previous studies (Dakhlaoui et al., 2020; Kelleher and Shaw, 2018). In detail, Dakhlaoui et al. (2020) compared runoff projection by three hydrological models with different ETp estimations in Northern Tunisia. They claimed that hydrological projections with different ETp estimations were similar, indicating the low sensitivity of hydrological models to different ETp inputs.

Overall, we found that the difference in runoff projection yielded by different ETp inputs was small for XAJ model. This could be partially explained by the fact that the difference in ETp estimates was trade off by difference in the calibrated model's parameters. For instance, the coefficient of deep evapotranspiration (C, shown in Table 2) was different as a result of the different ETp inputs. In other words, the calibration procedure of XAJ model with different ETp inputs also produced different parameters, thus trading off the difference in ETp inputs and yielding similar and good runoff simulation. Considering that some downscaled daily climate data (e.g. wind speed or relative humidity) are not always available to support the use of complicated ETp models (Oudin et al., 2005; Randall et al., 2007), the low sensitivity of XAJ model to ETp inputs is helpful to improve our confidence in the use of temperature-based or radiation-based ETp models in future runoff projection.

4.2. Runoff projections based on XAJ under future climate scenarios

This study predicted a general decrease in runoff under future climate scenarios, especially for spring and winter (Fig. 8). A decrease in runoff under a changing climate was reported by previous studies both in northeast and other parts of Australia (Eccles et al., 2021; Nguyen et al., 2020; Potter et al., 2010). For example, in southwest Western Australia, Barria et al. (2015) found that projected runoff by 2050–2080 would decrease by 10%-80% compared to runoff in 1970–2000. In a subtropical catchment of Queensland, Eccles et al. (2021) investigated the influence of climate change on runoff with climatic data downscaled from multi-model ensemble GCMs to drive a lumped conceptual hydrological model. They found that both high and mean streamflow were predicted to decrease. Note that their decreases in spring and winter were much larger than that in summer and autumn, which is consistent with our results.

Decrease in runoff was mainly caused by a decrease in rainfall though the increasing ETp also amplified the reduction (Fig. 6). We found that the R^2 between projected changes in runoff and rainfall was more than 0.86 (Fig. 9), which was much higher than its correlation with changes in ETp. This demonstrated that rainfall is the main driving factor in the change of projected runoff as reported by Charles et al. (2020). They claimed that increasing ETp would cause an additional reduction in runoff under a warming climate but changes in rainfall mainly determine the relative results. Similarly, Donohue et al. (2011) assessed the sensitivity of runoff to changes in precipitation and ETp based on Budyko's curve. They found that the change of precipitation caused larger change in runoff than that caused by the same change of ETp. In this study, the dominant role of rainfall in influencing runoff changes may also partially explain the low sensitivity of XAJ model to different ETp inputs.

Rainfall in North Johnstone catchment mainly occurs in summer and autumn (Fig. 2) (Zhang et al., 2020). By contrast, spring and winter are dry seasons for this catchment. The decreases of future rainfall and runoff will make these two seasons drier compared to baseline, which is likely to result in severe influence on the agricultural production and ecological functions in this catchment (Potter et al., 2010). For instance, the concentrations of nutrient and sediment may become larger as the flushing times tend to be longer apart with the dry seasons getting drier (Eccles et al., 2020; Eccles et al., 2021). Meanwhile, water consuming industries such as irrigators, forestry, and wetland in this region may face increasing demands and competition for water during these drier seasons (Petheram et al., 2012).

4.3. Uncertainty in runoff projection

We found that GCMs followed by interaction between GCMs and RCPs was the dominant source of uncertainty in projected runoff changes (Fig. 10). Similar results were reported by other studies. Lee et al. (2021) found that GCMs accounted for more than 45% of the total uncertainty in the projection of streamflow caused by hydrological model parameters, GCMs, and RCPs at Coastal Plain of the Chesapeake Bay watershed. At global scale, Arnell and Gosling (2013) reported that GCM-related uncertainty in hydrological projection was the largest among uncertainty caused by GCMs, emission scenarios, and the natural variability in hydrological regimes. The dominant role of GCMs played in the uncertainty in runoff projection may be attributed to the large uncertainty in rainfall projected by GCMs. According to Woldemeskel et al. (2016), GCMs accounted for around 90% of the uncertainty in rainfall projection. Therefore, the large uncertainty in rainfall projection caused by GCMs is likely to be transmitted to runoff projection as GCMs-downscaled rainfall is an essential input for XAJ model. As Petheram et al. (2012) reported in their study that the largest uncertainty in runoff projection was caused by rainfall projections from different GCMs. The high R^2 ($\geq$0.86) between change in runoff and rainfall in our study also support this conclusion. Different pathways of carbon dioxide, other anthropogenic emissions of greenhouse gases, aerosols and so on were associated with different RCPs and used as inputs to force GCMs to generate different climate simulations (Meinshausen et al., 2011). In other words, GCMs projections under different RCPs will result in different temperature and rainfall changes. Therefore, great contribution from the interaction between GCMs and RCPs to the uncertainty in runoff projection was not unexpected (Lee et al., 2021).

Compared to uncertainty caused by GCMs, uncertainty caused by ETp models was small though its contribution in autumn and winter became larger (Fig. 10). This finding may be explained by the fact that the projection of runoff is more influenced by rainfall instead of ETp (Charles et al., 2020; Rajulapati et al., 2020), as shown in Fig. 9 that R^2 between change in runoff and change in ETp was barely larger than 0.40. The uncertainty in runoff projection poses a great challenge for decision makers in taking measures to adapt to the possible water scarcity and stress. Though it is impossible to avoid uncertainty in climate projections, it is possible to reduce uncertainty from them (Hawkins and Sutton, 2011; Shoaib et al., 2018). For instance, narrowing down uncertainty from GCMs can be realized by screening the performance of GCMs and choosing GCMs which can well replicate historical observations for runoff projection. Wang et al. (2020b) quantified how many GCMs should be used to fully cover the uncertainty caused by them in runoff projection and concluded that at least 10 GCMs should be used. Therefore, attention should be paid both to the quality and to the quantity of GCMs used in runoff projection. In addition, another key requirement for reducing uncertainty in climate change impact assessment in hydrology is to better characterize climate change at the local level. The accuracy of climate system modeling has been improved over the last decades (Chen et al., 2021; Woldemeskel et al., 2016) with incorporating important physical processes, increasing models' complexities, and improving model's resolution. Chen et al. (2021) found that the latest Coupled Model Intercomparison Project Phases 6 (CMIP6) performed better in simulating extreme precipitation in Western North Pacific and East Asia.

4.4. Limitations of this study

In this study, we only used one hydrological model to assess the impacts of climate change on runoff. Previous studies demonstrated that the direction of projected future runoff change by different hydrological models for a certain catchment is likely to be consistent (Pechlivanidis et al., 2016; Teng et al., 2012). However, it is very important to adopt multiple hydrology models to investigate the magnitude of runoff change under future climate. In addition, as only one hydrological model was used in this study, the contribution of hydrological models to uncertainty in runoff projection was not investigated. Some studies concluded that uncertainty caused by hydrological models was small compared with that caused by GCMs and RCPs (Aryal et al., 2019; Bosshard et al., 2013; Gosling and Arnell, 2011). For example, Teng et al. (2012) adopted five hydrological models with downscaled climate data from 15 GCMs to investigate climate change impact on runoff in southeastern Australia and analyzed the uncertainty caused by different sources. They found that the uncertainty in runoff change caused by GCMs with a certain hydrological model was around four or five times larger than the uncertainty caused by hydrological models with a certain GCM. Even so, it is still necessary to include this factor in the future study to avoid the possible underestimation of the total uncertainty related with runoff projection (Bosshard et al., 2013). Note that our results were specific to a certain catchment projected by XAJ model. It may yield discordant conclusions when different catchments or hydrological models are used. For instance, Jung et al. (2012) claimed that uncertainty in hydrological projection at rain-dominated basin was different with that in the snow-dominated basin. Therefore, it is necessary for future research to consider more hydrological models to investigate the influence of ETp models at multiple contrasting catchments.

5. Conclusions

We investigated the influence of different ETp inputs on runoff simulation and projection with XAJ model in North Johnstone catchment, northeast Australia. Meanwhile, we quantified the contribution of GCMs, RCPs, ETp models, and their interaction to the uncertainty in runoff projection with a method of three-way analysis of variance. Our findings indicated that XAJ model performed well in runoff simulation, in the study catchment. We found that XAJ model with different ETp inputs projected similar decreases in spring and winter runoff while a small change in summer and autumn runoff. It is feasible to adopt simple empirical ETp models to project runoff especially when some downscaled climate data (e.g., winds and vapour pressure) are not available. We also found that GCMs and its interaction with RCPs contributed the most to the uncertainty in runoff projection. This highlighted the necessity to adopt multiple GCMs and RCPs to comprehensively project the potential influence of climate change on runoff. Our finding also provide a way forward to narrow down the uncertainty in runoff projection.

Note that all our results are specific to XAJ model at a wet tropical catchment. In future studies, we expect to employ more hydrological models with different ETp inputs driven by the latest CMIP6 climatic data to quantify the uncertainty on runoff projection at various catchments.

CRediT authorship contribution statement

Lijie Shi: Conceptualization, Data curation, Formal analysis, Methodology, Visualization, Writing – original draft, Writing – review & editing. **Puyu Feng:** Data curation, Investigation, Formal analysis, Software, Writing – original draft. **Bin Wang:** Conceptualization, Methodology, Supervision. **De Li Liu:** Data curation, Methodology, Resources, Supervision. **Hong Zhang:** Data curation, Software. **Jiandong Liu:** Writing – review & editing. **Qiang Yu:** Funding acquisition, Investigation, Resources, Project administration, Supervision.

Declaration of Competing Interest

The authors declare that they have no known competing financial interests or personal relationships that could have appeared to influence the work reported in this paper.

Acknowledgements

The first author acknowledges a scholarship from the Chinese Scholarship Council, and the NSW Department of Primary Industries provided office facilities for conducting this work. We acknowledge the support from Natural Science Foundation of China (No.41961124006, 41730645) and US National Science Foundation (1903722). We also appreciate the Scientific Information for Land Owners and the Bureau of Meteorology for the access of climatic data used in this study. Bernie Dominiak reviewed an early version of the manuscript. We are very grateful to three reviewers and editor for their very thorough and helpful comments which greatly improved our manuscript.

Appendix A. Supplementary data

Supplementary data to this article can be found online at https://doi.org/10.1016/j.jhydrol.2022.128042.

References

Allan, R.P., Barlow, M., Byrne, M.P., Cherchi, A., Douville, H., Fowler, H.J., Gan, T.Y., Pendergrass, A.G., Rosenfeld, D., Swann, A.L.S., Wilcox, L.J., Zolina, O., 2020. Advances in understanding large-scale responses of the water cycle to climate change. Ann. N. Y. Acad. Sci. 1472 (1), 49–75.

Allen, R.G., Pereira, L.S., Raes, D., Smith, M., 1998. Crop evapotranspiration - Guidelines for computing Crop Water Requirements. FAO Irrigation & Drainage Paper 56, Rome, Italy.

Almorox, J., Quej, V.H., Martí, P., 2015. Global performance ranking of temperature-based approaches for evapotranspiration estimation considering Köppen climate classes. J. Hydrol. 528, 514–522. https://doi.org/10.1016/j.jhydrol.2015.06.057.

Arnell, N.W., 2011. Uncertainty in the relationship between climate forcing and hydrological response in UK catchments. Hydrol. Earth Syst. Sci. 15 (3), 897–912. https://doi.org/10.5194/hess-15-897-2011.

Arnell, N.W., Gosling, S.N., 2013. The impacts of climate change on river flow regimes at the global scale. J. Hydrol. 486, 351–364. https://doi.org/10.1016/j.jhydrol.2013.02.010.

Aryal, A., Shrestha, S., Babel, M.S., 2019. Quantifying the sources of uncertainty in an ensemble of hydrological climate-impact projections. Theor. Appl. Climatol. 135 (1), 193–209. https://doi.org/10.1007/s00704-017-2359-3.

Bae, D.-H., Jung, I.-W., Lettenmaier, D.P., 2011. Hydrologic uncertainties in climate change from IPCC AR4 GCM simulations of the Chungju Basin, Korea. J. Hydrol. 401 (1), 90–105. https://doi.org/10.1016/j.jhydrol.2011.02.012.

Bai, P., Liu, X., Yang, T., Li, F., Liang, K., Hu, S., Liu, C., 2016. Assessment of the influences of different potential evapotranspiration inputs on the performance of monthly hydrological models under different climatic conditions. J. Hydrometeorol. 17 (8), 2259–2274.

Barria, P., Walsh, K.J.E., Peel, M.C., Karoly, D., 2015. Uncertainties in runoff projections in southwestern Australian catchments using a global climate model with perturbed physics. J. Hydrol. 529, 184–199. https://doi.org/10.1016/j.jhydrol.2015.07.040.

Bosshard, T., Carambia, M., Goergen, K., Kotlarski, S., Krahe, P., Zappa, M., Schär, C., 2013. Quantifying uncertainty sources in an ensemble of hydrological climate-impact projections. Water Resour. Res. 49 (3), 1523–1536. https://doi.org/10.1029/2011wr011533.

Charles, S.P., Chiew, F.H.S., Potter, N.J., Zheng, H., Fu, G., Zhang, L.u., 2020. Impact of downscaled rainfall biases on projected runoff changes. Hydrol. Earth Syst. Sci. 24 (6), 2981–2997. https://doi.org/10.5194/hess-24-2981-2020.

Chegwidden, O.S., Nijssen, B., Rupp, D.E., Arnold, J.R., Clark, M.P., Hamman, J.J., Kao, S.-C., Mao, Y., Mizukami, N., Mote, P.W., Pan, M., Pytlak, E., Xiao, M.u., 2019. How Do Modeling Decisions Affect the Spread Among Hydrologic Climate Change Projections? Exploring a Large Ensemble of Simulations Across a Diversity of Hydroclimates. Earth's Future 7 (6), 623–637. https://doi.org/10.1029/2018EF001047.

Chen, C.-A., Hsu, H.-H., Liang, H.-C., 2021. Evaluation and comparison of CMIP6 and CMIP5 model performance in simulating the seasonal extreme precipitation in the Western North Pacific and East Asia. Weather Clim. Extremes 31, 100303. https://doi.org/10.1016/j.wace.2021.100303.

Chen, Y.-R., Yu, B., 2015. Impact assessment of climatic and land-use changes on flood runoff in southeast Queensland. Evaluation de l'impact des changements climatiques et de l'utilisation des terres sur l'écoulement de crue dans le Sud-Est du Queensland. 60 (10), 1759–1769. https://doi.org/10.1080/02626667.2014.945938.

Chiew, F., Zheng, H., Potter, N., 2018. Rainfall-runoff modelling considerations to predict streamflow characteristics in ungauged catchments and under climate change. Water 10 (10), 1319. https://doi.org/10.3390/w10101319.

Dakhlaoui, H., Seibert, J., Hakala, K., 2020. Sensitivity of discharge projections to potential evapotranspiration estimation in Northern Tunisia. Reg. Environ. Change 20 (2), 34. https://doi.org/10.1007/s10113-020-01615-8.

Devi, G.K., Ganasri, B.P., Dwarakish, G.S., 2015. A Review on Hydrological Models. Aquat. Procedia 4, 1001–1007. https://doi.org/10.1016/j.aqpro.2015.02.126.

Do, H.X., Westra, S., Leonard, M., 2017. A global-scale investigation of trends in annual maximum streamflow. J. Hydrol. 552, 28–43. https://doi.org/10.1016/j.jhydrol.2017.06.015.

Donohue, R.J., Roderick, M.L., McVicar, T.R., 2011. Assessing the differences in sensitivities of runoff to changes in climatic conditions across a large basin. J. Hydrol. 406 (3), 234–244. https://doi.org/10.1016/j.jhydrol.2011.07.003.

Eccles, R., Zhang, H., Hamilton, D., Maxwell, P., 2020. Trends in water quality in a subtropical Australian river-estuary system: responses to damming, climate variability and wastewater discharges. J Environ Manage 269, 110796. https://doi.org/10.1016/j.jenvman.2020.110796.

Eccles, R., Zhang, H., Hamilton, D., Trancoso, R., Syktus, J., 2021. Impacts of climate change on streamflow and floodplain inundation in a coastal subtropical catchment. Adv. Water Resour. 147, 103825 https://doi.org/10.1016/j.advwatres.2020.103825.

Fang, D., et al., 2020. Combined effects of urbanization and climate change on watershed evapotranspiration at multiple spatial scales. J. Hydrol. 587, 124869. https://doi.org/10.1016/j.jhydrol.2020.124869.

Feng, Y., Cui, N., Zhao, L., Hu, X., Gong, D., 2016. Comparison of ELM, GANN, WNN and empirical models for estimating reference evapotranspiration in humid region of Southwest China. J. Hydrol. 536, 376–383. https://doi.org/10.1016/j.jhydrol.2016.02.053.

Fowler, K., Coxon, G., Freer, J., Peel, M., Wagener, T., Western, A., Woods, R., Zhang, L.u., 2018. Simulating runoff under changing climatic conditions: a framework for model improvement. Water Resour. Res. 54 (12), 9812–9832. https://doi.org/10.1029/2018WR023989.

Freni, G., Mannina, G., Viviani, G., 2009. Urban runoff modelling uncertainty: Comparison among Bayesian and pseudo-Bayesian methods. Environ. Modell. Software 24 (9), 1100–1111. https://doi.org/10.1016/j.envsoft.2009.03.003.

Ghasemizade, M., Schirmer, M., 2013. Subsurface flow contribution in the hydrological cycle: lessons learned and challenges ahead—a review. Environ. Earth Sci. 69 (2), 707–718. https://doi.org/10.1007/s12665-013-2329-8.

Gosling, S.N., Arnell, N.W., 2011. Simulating current global river runoff with a global hydrological model: model revisions, validation, and sensitivity analysis. Hydrol. Process. 25 (7), 1129–1145. https://doi.org/10.1002/hyp.7727.

Guo, D., Westra, S., Maier, H.R., 2017a. Impact of evapotranspiration process representation on runoff projections from conceptual rainfall-runoff models. Water Resour. Res. 53 (1), 435–454. https://doi.org/10.1002/2016WR019627.

Guo, D., Westra, S., Maier, H.R., 2017b. Sensitivity of potential evapotranspiration to changes in climate variables for different Australian climatic zones. Hydrol. Earth Syst. Sci. 21 (4), 2107–2126. https://doi.org/10.5194/hess-21-2107-2017.

Haerter, J.O., Hagemann, S., Moseley, C., Piani, C., 2011. Climate model bias correction and the role of timescales. Hydrol. Earth Syst. Sci. 15 (3), 1065–1079. https://doi.org/10.5194/hess-15-1065-2011.

Hawkins, E., Sutton, R., 2011. The potential to narrow uncertainty in projections of regional precipitation change. Clim. Dyn. 37 (1), 407–418. https://doi.org/10.1007/s00382-010-0810-6.

Im, E.-S., Jung, I.-W., Chang, H., Bae, D.-H., Kwon, W.-T., 2009. Hydroclimatological response to dynamically downscaled climate change simulations for Korean basins. Clim. Change 100 (3–4), 485–508. https://doi.org/10.1007/s10584-009-9691-2.

Irmak, S., Kabenge, I., Skaggs, K.E., Mutiibwa, D., 2012. Trend and magnitude of changes in climate variables and reference evapotranspiration over 116-yr period in the Platte River Basin, central Nebraska–USA. J. Hydrol. 420–421, 228–244. https://doi.org/10.1016/j.jhydrol.2011.12.006.

Islam, S.A., Bari, M.A., Anwar, A.H.M.F., 2014. Hydrologic impact of climate change on Murray-Hotham catchment of Western Australia: a projection of rainfall–runoff for future water resources planning. Hydrol. Earth Syst. Sci. 18 (9), 3591–3614. https://doi.org/10.5194/hess-18-3591-2014.

Jeffrey, S.J., Carter, J.O., Moodie, K.B., Beswick, A.R., 2001. Using spatial interpolation to construct a comprehensive archive of Australian climate data. Environ. Modell. Software 16 (4), 309–330. https://doi.org/10.1016/S1364-8152(01)00008-1.

Jung, I.-W., Moradkhani, H., Chang, H., 2012. Uncertainty assessment of climate change impacts for hydrologically distinct river basins. J. Hydrol. 466–467, 73–87. https://doi.org/10.1016/j.jhydrol.2012.08.002.

Kelleher, C.A., Shaw, S.B., 2018. Is ET often oversimplified in hydrologic models? Using long records to elucidate unaccounted for controls on ET. J. Hydrol. 557, 160–172. https://doi.org/10.1016/j.jhydrol.2017.12.018.

Knutti, R., Sedláček, J., 2012. Robustness and uncertainties in the new CMIP5 climate model projections. Nature Climate Change 3, 369. https://www.nature.com/articles/nclimate1716#supplementary-information. https://doi.org/10.1038/nclimate1716.

Kuchment, L.S., 2004. THE HYDROLOGICAL CYCLE AND HUMAN IMPACT ON IT, in Water Resources Management, [Eds. Arjen Y. Hoekstra, and Hubert H.G. Savenije], in Encyclopedia of Life Support Systems (EOLSS), Developed under the Auspices of the UNESCO. Eolss Publishers, Oxford, UK, [http://www.eolss.net].

Kumar, K.K., Kumar, K.R., Rakhecha, P., 1987. Comparison of Penman and Thornthwaite methods of estimating potential evapotranspiration for Indian conditions. Theor. Appl. Climatol. 38 (3), 140–146.

Lee, S., et al., 2021. Uncertainty assessment of multi-parameter, multi-GCM, and multi-RCP simulations for streamflow and non-floodplain wetland (NFW) water storage. J. Hydrol. 600, 126564. https://doi.org/10.1016/j.jhydrol.2021.126564.

Li, Z., Li, Q., Wang, J., Feng, Y., Shao, Q., 2020. Impacts of projected climate change on runoff in upper reach of Heihe River basin using climate elasticity method and GCMs. Sci. Total Environ. 716, 137072 https://doi.org/10.1016/j.scitotenv.2020.137072.

Li, H., Zhang, Y., Vaze, J., Wang, B., 2012. Separating effects of vegetation change and climate variability using hydrological modelling and sensitivity-based approaches. J. Hydrol. 420–421, 403–418. https://doi.org/10.1016/j.jhydrol.2011.12.033.

Li, H., Zhang, Y., Chiew, F.H.S., Xu, S., 2009. Predicting runoff in ungauged catchments by using Xinanjiang model with MODIS leaf area index. J. Hydrol. 370 (1), 155–162. https://doi.org/10.1016/j.jhydrol.2009.03.003.

Li, H., Zhang, Y., 2017. Regionalising rainfall-runoff modelling for predicting daily runoff: Comparing gridded spatial proximity and gridded integrated similarity approaches against their lumped counterparts. J. Hydrol. 550, 279–293. https://doi.org/10.1016/j.jhydrol.2017.05.015.

Liu, D.L., Zuo, H., 2012. Statistical downscaling of daily climate variables for climate change impact assessment over New South Wales, Australia. Climatic Change 115 (3), 629–666. https://doi.org/10.1007/s10584-012-0464-y.

Meinshausen, M., Smith, S.J., Calvin, K., Daniel, J.S., Kainuma, M.L.T., Lamarque, J.-F., Matsumoto, K., Montzka, S.A., Raper, S.C.B., Riahi, K., Thomson, A., Velders, G.J.M., van Vuuren, D.P.P., 2011. The RCP greenhouse gas concentrations and their extensions from 1765 to 2300. Clim. Change 109 (1-2), 213–241. https://doi.org/10.1007/s10584-011-0156-z.

Montaldo, N., Oren, R., 2018. Changing Seasonal Rainfall Distribution With Climate Directs Contrasting Impacts at Evapotranspiration and Water Yield in the Western Mediterranean Region. Earth's Future 6 (6), 841–856. https://doi.org/10.1029/2018ef000843.

Morim, J., Hemer, M., Wang, X.L., Cartwright, N., Trenham, C., Semedo, A., Young, I., Bricheno, L., Camus, P., Casas-Prat, M., Erikson, L.i., Mentaschi, L., Mori, N., Shimura, T., Timmermans, B., Aarnes, O., Breivik, Ø., Behrens, A., Dobrynin, M., Menendez, M., Staneva, J., Wehner, M., Wolf, J., Kamranzad, B., Webb, A., Stopa, J., Andutta, F., 2019. Robustness and uncertainties in global multivariate wind-wave climate projections. Nat. Clim. Change 9 (9), 711–718. https://doi.org/10.1038/s41558-019-0542-5.

Nguyen, H., Mehrotra, R., Sharma, A., 2020. Assessment of Climate Change Impacts on Reservoir Storage Reliability, Resilience, and Vulnerability Using a Multivariate Frequency Bias Correction Approach. Water Resour. Res. 56 (2) https://doi.org/10.1029/2019wr026022.

Oudin, L., Hervieu, F., Michel, C., Perrin, C., Andréassian, V., Anctil, F., Loumagne, C., 2005. Which potential evapotranspiration input for a lumped rainfall–runoff model? J. Hydrol. 303 (1-4), 290–306. https://doi.org/10.1016/j.jhydrol.2004.08.026.

Pan, S., et al., 2015. Responses of global terrestrial evapotranspiration to climate change and increasing atmospheric CO2 in the 21st century. Earth's Future 3 (1), 15–35. https://doi.org/10.1002/2014EF000263.

Pechlivanidis, I.G., Arheimer, B., Donnelly, C., Hundecha, Y., Huang, S., Aich, V., Samaniego, L., Eisner, S., Shi, P., 2016. Analysis of hydrological extremes at different hydro-climatic regimes under present and future conditions. Clim. Change 141 (3), 467–481. https://doi.org/10.1007/s10584-016-1723-0.

Petheram, C., Rustomji, P., McVicar, T.R., Cai, WenJu, Chiew, F.H.S., Vleeshouwer, J., Van Niel, T.G., Li, LingTao, Cresswell, R.G., Donohue, R.J., Teng, J., Perraud, J.-M., 2012. Estimating the Impact of Projected Climate Change on Runoff across the Tropical Savannas and Semiarid Rangelands of Northern Australia. J. Hydrometeorol. 13 (2), 483–503. https://doi.org/10.1175/JHM-D-11-062.1.

Potter, N.J., Chiew, F.H.S., Frost, A.J., 2010. An assessment of the severity of recent reductions in rainfall and runoff in the Murray-Darling Basin. J. Hydrol. 381 (1–2), 52–64. https://doi.org/10.1016/j.jhydrol.2009.11.025.

Priestley, C.H.B., Taylor, R.J., 1972. On the assessment of surface heat flux and evaporation using large-scale parameters. Mon. Weather Rev. 100 (2), 81–92. https://doi.org/10.1175/1520-0493(1972)100<0081:Otaosh>2.3.Co;2.

Rafiei, V., Ghahramani, A., An-Vo, D.-A., Mushtaq, S., 2020. Modelling hydrological processes and identifying soil erosion sources in a tropical catchment of the great barrier reef using SWAT. Water 12 (8), 2179. https://doi.org/10.3390/w12082179.

Rajulapati, C.R., Papalexiou, S.M., Clark, M.P., Razavi, S., Tang, G., Pomeroy, J.W., 2020. Assessment of extremes in global precipitation products: how reliable are

they? J. Hydrometeorol. 21 (12), 2855–2873. https://doi.org/10.1175/jhm-d-20-0040.1.
Randall, D.A., et al., 2007. Climate models and their evaluation, Climate change 2007: The physical science basis. Contribution of Working Group I to the Fourth Assessment Report of the IPCC (FAR). Cambridge University Press, pp. 589–662.
Riegger, J., Tourian, M.J., 2014. Characterization of runoff-storage relationships by satellite gravimetry and remote sensing. Water Resour. Res. 50 (4), 3444–3466. https://doi.org/10.1002/2013wr013847.
Roy, D.K., Barzegar, R., Quilty, J., Adamowski, J., 2020. Using ensembles of adaptive neuro-fuzzy inference system and optimization algorithms to predict reference evapotranspiration in subtropical climatic zones. J. Hydrol. 591, 125509.
Samani, Z., 2000. Estimating solar radiation and evapotranspiration using minimum climatological data. J. Irrig. Drain. Eng. 126 (4), 265–267. https://doi.org/10.1061/(ASCE)0733-9437(2000)126:4(265).
Seiller, G., Anctil, F., 2014. Climate change impacts on the hydrologic regime of a Canadian river: comparing uncertainties arising from climate natural variability and lumped hydrological model structures. Hydrol. Earth Syst. Sci. 18 (6), 2033–2047. https://doi.org/10.5194/hess-18-2033-2014.
Seiller, G., Anctil, F., 2016. How do potential evapotranspiration formulas influence hydrological projections? Hydrol. Sci. J. 61 (12), 2249–2266. https://doi.org/10.1080/02626667.2015.1100302.
Senent-Aparicio, J., Pérez-Sánchez, J., Carrillo-García, J., Soto, J., 2017. Using SWAT and Fuzzy TOPSIS to Assess the Impact of Climate Change in the Headwaters of the Segura River Basin (SE Spain). water 9 (2). https://doi.org/10.3390/W9020149.
Shen, Y., Oki, T., Kanae, S., Hanasaki, N., Utsumi, N., Kiguchi, M., 2014. Projection of future world water resources under SRES scenarios: an integrated assessment. Hydrol. Sci. J. 59 (10), 1775–1793. https://doi.org/10.1080/02626667.2013.862338.
Shi, L., et al., 2020. Projecting potential evapotranspiration change and quantifying its uncertainty under future climate scenarios: A case study in southeastern Australia. J. Hydrol. 584, 124756. https://doi.org/10.1016/j.jhydrol.2020.124756.
Shoaib, S.A., Marshall, L., Sharma, A., 2018. Attributing uncertainty in streamflow simulations due to variable inputs via the Quantile Flow Deviation metric. Adv. Water Resour. 116, 40–55. https://doi.org/10.1016/j.advwatres.2018.01.022.
Teng, J., Vaze, J., Chiew, F.H.S., Wang, B., Perraud, J.-M., 2012. Estimating the Relative Uncertainties Sourced from GCMs and Hydrological Models in Modeling Climate Change Impact on Runoff. J. Hydrometeorol. 13 (1), 122–139. https://doi.org/10.1175/jhm-d-11-058.1.
Teng, J., Potter, N.J., Chiew, F.H.S., Zhang, L., Wang, B., Vaze, J., Evans, J.P., 2015. How does bias correction of regional climate model precipitation affect modelled runoff? Hydrol. Earth Syst. Sci. 19 (2), 711–728. https://doi.org/10.5194/hess-19-711-2015.
Tian, Y., Xu, Y.-P., Zhang, X.-J., 2013. Assessment of Climate Change Impacts on River High Flows through Comparative Use of GR4J, HBV and Xinanjiang Models. Water Resour. Manage. 27 (8), 2871–2888. https://doi.org/10.1007/s11269-013-0321-4.
Vaze, J., Teng, J., 2011. Future climate and runoff projections across New South Wales, Australia: results and practical applications. Hydrol. Process. 25 (1), 18–35. https://doi.org/10.1002/hyp.7812.
Vetter, T., Reinhardt, J., Flörke, M., van Griensven, A., Hattermann, F., Huang, S., Koch, H., Pechlivanidis, I.G., Plötner, S., Seidou, O., Su, B., Vervoort, R.W., Krysanova, V., 2017. Evaluation of sources of uncertainty in projected hydrological changes under climate change in 12 large-scale river basins. Clim. Change 141 (3), 419–433. https://doi.org/10.1007/s10584-016-1794-y.
Wang, H.M., Chen, J., Xu, C.Y., Zhang, J., Chen, H., 2020b. A Framework to Quantify the Uncertainty Contribution of GCMs Over Multiple Sources in Hydrological Impacts of Climate Change. Earth's. Future 8 (8). https://doi.org/10.1029/2020ef001602.
Wang, B., Feng, P., Liu, D.L., O'Leary, G.J., Macadam, I., Waters, C., Asseng, S., Cowie, A., Jiang, T., Xiao, D., Ruan, H., He, J., Yu, Q., 2020a. Sources of uncertainty for wheat yield projections under future climate are site-specific. Nature Food 1 (11), 720–728. https://doi.org/10.1038/s43016-020-00181-w.
Woldemeskel, F.M., Sharma, A., Sivakumar, B., Mehrotra, R., 2016. Quantification of precipitation and temperature uncertainties simulated by CMIP3 and CMIP5 models. J. Geophys. Res.: Atmos. 121 (1), 3–17. https://doi.org/10.1002/2015JD023719.
Xing, W., Wang, W., Zou, S., Deng, C., 2018. Projection of future runoff change using climate elasticity method derived from Budyko framework in major basins across China. Global Planet. Change 162, 120–135. https://doi.org/10.1016/j.gloplacha.2018.01.006.
Yan, Z., Zhou, Z., Liu, J., Han, Z., Gao, G.e., Jiang, X., 2020. Ensemble Projection of Runoff in a Large-Scale Basin: Modeling With a Global BMA Approach. Water Resour. Res. 56 (7) https://doi.org/10.1029/2019wr026134.
Yang, Y., Liu, D.L., Anwar, M.R., O'Leary, G., Macadam, I., Yang, Y., 2016. Water use efficiency and crop water balance of rainfed wheat in a semi-arid environment: sensitivity of future changes to projected climate changes and soil type. Theor. Appl. Climatol. 123 (3-4), 565–579. https://doi.org/10.1007/s00704-015-1376-3.
Yang, H., Yang, D., 2011. Derivation of climate elasticity of runoff to assess the effects of climate change on annual runoff. Water Resour. Res. 47 (7) https://doi.org/10.1029/2010wr009287.
Yip, S., Ferro, C.A.T., Stephenson, D.B., Hawkins, E., 2011. A simple, coherent framework for partitioning uncertainty in climate predictions. J. Clim. 24 (17), 4634–4643. https://doi.org/10.1175/2011jcli4085.1.
Zhang, H., Wang, B., Liu, D.L., Zhang, M., Feng, P., Cheng, L., Yu, Q., Eamus, D., 2019. Impacts of future climate change on water resource availability of eastern Australia: A case study of the Manning River basin. J. Hydrol. 573, 49–59. https://doi.org/10.1016/j.jhydrol.2019.03.067.
Zhang, H., Wang, B., Liu, D.L., Zhang, M., Leslie, L.M., Yu, Q., 2020. Using an improved SWAT model to simulate hydrological responses to land use change: a case study of a catchment in tropical Australia. J. Hydrol. 585, 124822.
Zhao, R.-J., 1992. The Xinanjiang model applied in China. J. Hydrol. 135 (1), 371–381. https://doi.org/10.1016/0022-1694(92)90096-E.
Zheng, H., Yu, G., Wang, Q., Zhu, X., Yan, J., Wang, H., Shi, P., Zhao, F., Li, Y., Zhao, L., Zhang, J., Wang, Y., 2017. Assessing the ability of potential evapotranspiration models in capturing dynamics of evaporative demand across various biomes and climatic regimes with ChinaFLUX measurements. J. Hydrol. 551, 70–80. https://doi.org/10.1016/j.jhydrol.2017.05.056.